Global Biogeochemical Cycles

RESEARCH ARTICLE
10.1029/2018GB006146

Fertilization of the Northwest Pacific Ocean by East Asia Air Pollutants

Chao Zhang[1,2], Akinori Ito[3], Zongbo Shi[2,4], Maki Noguchi Aita[3], Xiaohong Yao[1], Qiang Chu[1,5], Jinhui Shi[1], Xiang Gong[6], and Huiwang Gao[1,7]

[1]Key Laboratory of Marine Environment and Ecology, Ministry of Education of China, Ocean University of China, Qingdao, China, [2]School of Geography, Earth and Environmental Sciences, University of Birmingham, Birmingham, UK, [3]Yokohama Institute for Earth Sciences, JAMSTEC, Yokohama, Japan, [4]Institute of Surface Earth System Science, Tianjin University, Tianjin, China, [5]Laboratory of Environmental Protection in Water Transport Engineering, Tianjin Research Institute for Water Transport Engineering, Ministry of Transport, Tianjin, China, [6]School of Mathematics and Physics, Qingdao University of Science and Technology, Qingdao, China, [7]Laboratory for Marine Ecology and Environmental Sciences, Qingdao National Laboratory for Marine Science and Technology, Qingdao, China

Abstract Haze particles as a key air pollutant contain high level of toxins, which were hypothesized to inhibit phytoplankton growth when deposited to the ocean, and thus indirectly affect the climate. However, field observations have yet to provide conclusive evidence to confirm this hypothesis. Onboard microcosm experiments in the Northwest Pacific Ocean (NWPO) show that haze particles collected at the East Asia continent had an inhibition impact on phytoplankton growth only when at very high particle loading (2 mg/L). In contrast, haze particles at low and medium loadings (0.03–0.6 mg/L) stimulated phytoplankton growth and shifted phytoplankton size structure toward larger cells, primarily due to the supply of inorganic nitrogen nutrients from the particles. Model simulations showed that haze particle loading in NWPO surface seawater was usually more than an order of magnitude lower than 2 mg/L. This indicates that haze particles are unlikely to cause harm but to stimulate phytoplankton growth in the nitrogen-limited NWPO. Ocean biogeochemical modeling further shows that deposited nitrogen significantly enhanced surface ocean chlorophyll *a* concentration in the winter and spring of 2014. Overall, these results demonstrate that haze particles stimulate rather than inhibit primary production in the NWPO.

Plain Language Summary Increasing anthropogenic emissions of air pollutants from fast-developing East Asia leads to increasing deposition of aerosol particles to the Northwest Pacific Ocean (NWPO). Such particles contain both nutrients such as nitrogen and phosphorus and toxins such as copper and organic pollutants to the marine phytoplankton, which have contrasting effects on marine ecosystems and carbon uptake. However, the actual impact remains unknown. Detailed onboard incubation experiments confirm that Chinese haze particles have an overall stimulation effects on phytoplankton under representative ocean conditions in NWPO. Toxicity to phytoplankton is only observed when the added haze particle concentration is unrealistically high. Simulations suggest that nitrogen in the atmospheric deposition contributes significantly to the surface chlorophyll *a* concentration in NWPO and enhances carbon fixation, which indirectly offsets global warming.

Key Points:
- Toxicity of haze particle is observed only at unrealistically high concentrations (2 mg/L) in the seawater
- Haze particles at low to medium loading (0.03–0.6 mg/L) stimulated phytoplankton growth and shifted phytoplankton size structure toward larger cells
- Deposition of haze particles under realistic environmental conditions stimulates primary production in the Northwest Pacific Ocean

Supporting Information:
- Supporting Information S1
- Figure S1
- Table S1

Correspondence to:
Z. Shi and H. Gao,
z.shi@bham.ac.uk;
hwgao@ouc.edu.cn

Citation:
Zhang, C., Ito, A., Shi, Z., Aita, M. N., Yao, X., Chu, Q., et al. (2019). Fertilization of the Northwest Pacific Ocean by East Asia air pollutants. *Global Biogeochemical Cycles*, *33*, 690–702. https://doi.org/10.1029/2018GB006146

Received 4 DEC 2018
Accepted 25 APR 2019
Accepted article online 6 MAY 2019
Published online 11 JUN 2019
Corrected 16 JUL 2019

This article was corrected on 16 JUL 2019. See the end of the full text for details.

1. Introduction

With the rapid growth of population and economy, air pollutant emissions in China contribute a large fraction of the global emissions (Zhao et al., 2012). Such high emissions lead to increasing occurrence of haze events (often defined as daily fine particle $PM_{2.5}$ concentration > 75 μg m^{-3} and visibility less than 5 km for over 6 hr) across China, increasing from ~20 days per year (d/year) in the 1990s to 40 d/year in the 2000s and to ~90.5 d/year in 2013 (Su et al., 2014). Haze pollution causes visibility degradation that influences transport and economy (Tie et al., 2016). It also affects the climate directly via aerosol radiation and indirectly by aerosol-cloud interaction (Zhang et al., 2015). Furthermore, fine haze particles cause respiratory and cardiovascular system diseases (Gao et al., 2015) and contribute to millions of premature deaths per year. Therefore, haze pollution has become a severe public health problem associated with industrialization and urbanization in China.

A large fraction of particles will be transported out of the continent and deposited to the oceans. This can supply a range of chemical compounds, some of which are toxins, such as copper (Cu) and cadmium (Cd) (Jordi et al., 2012; Miao et al., 2005; Paytan et al., 2009) while others are macronutrient (e.g., N, P) and micronutrient (e.g., Fe, Ito et al., 2019; Liu et al., 2013; Shi et al., 2012) to phytoplankton. Toxins have the potential to inhibit phytoplankton growth. For example, Paytan et al. (2009) showed that atmospheric aerosol inhibited the growth of pico-eukaryotes and *Synechococcus* in the northern Red Sea; Jordi et al. (2012) found a positive correlation of higher Cu concentration in the atmosphere with lower Chlorophyll *a* (Chl *a*) in the East Mediterranean Sea although this does not prove a causal relationship. Both studies hypothesized that the toxicity effect is due to high copper concentrations in atmospheric aerosols. Considering the increasing emissions of toxins to the atmosphere including heavy metals (e.g., copper and cadmium, Jordi et al., 2012; Miao et al., 2005; Paytan et al., 2009) and organic pollutants (e.g., phenanthrene and pyrene, Echeveste et al., 2010), toxicity of aerosol deposition has become an increasing concern. However, the hypothesis of aerosol toxicity to phytoplankton remains to be tested.

On the other hand, nutrients in atmospheric deposition have the potential to stimulate phytoplankton growth in surface oceans (Boyd et al., 2007; Li et al., 2017; Liu et al., 2013). Many previous ship-borne incubation and mesocosm experiments showed stimulation effects on phytoplankton growth, either by directly providing nutrients or by enhancing nitrogen fixation after addition of aerosol samples, including Asian dust (Chu et al., 2018; Krom et al., 2016; Liu et al., 2013; Meng et al., 2016; Mills et al., 2004; Zhang et al., 2018). Previous studies including Duce et al. (2008), Mahowald (2011), and Martino et al. (2014) also calculated the additional uptake of carbon dioxide (and thus climate effect) due to the nitrogen fertilization effects. However, these calculations did not consider the potential toxicity of aerosols to phytoplankton. If the aerosol toxicity is significant, those calculations would be inaccurate. Therefore, understanding the overall impact of atmospheric deposition on the marine phytoplankton is of paramount importance before we can quantify the effects of atmospheric depositions on the Earth system.

Northwest Pacific Ocean (NWPO) is an ocean area of particular interest because it is not only affected by mineral dust deposition (containing Fe and P as nutrients and low concentration of toxic metals) as well as increasing anthropogenic emissions from northeast Asian countries (including high concentration of nutrients such as NO_3^- and NH_4^+ as well as high loading of toxins such as heavy metals and organic pollutants, Kim et al., 2014; Martino et al., 2014; Miao et al., 2005; Paytan et al., 2009; Shi et al., 2012). There is evidence that the nutrients supplied by dust deposition can stimulate primary productivity in the NWPO (Chu et al., 2018; Meng et al., 2016; Shi et al., 2012; Zhang et al., 2018). Meanwhile, in contrast with the preindustrial time, the modern NWPO has been subjected to increasing deposition of trace metals that may cause toxicity to the phytoplankton (Paytan et al., 2009; Wang et al., 2017). However, the system is complex as Cu is also an important nutrient and its toxicity may be alleviated by soluble aerosol Fe or by increased complexation effect with organic matter (Meng et al., 2016; Paytan et al., 2009; Wang et al., 2017). How the NWPO system will respond to this complex nutrient and toxin inputs remains to be elucidated.

The purpose of this study is to determine the impact of haze particle deposition on phytoplankton growth in the surface seawater of NWPO (10–41°N, 109–160°E). To this aim, we carried out nine sets of microcosm experiments on board R/V *Dongfanghong* 2 by adding varying concentrations of haze particles and various nutrients (N, P, and Fe) into the incubation bottles filled with collected surface seawater at nine stations during the spring cruises of 2014, 2015, and 2016. Measurements of total Chl *a*, sized-fractioned Chl *a*, and nutrients over the duration of the incubations were used to examine the temporal differences between control (no addition) and various treatment incubations. We also carried out aerosol model simulations to calculate the deposition fluxes of particles over the regions in the winter and spring, which were used to estimate the concentrations of haze particles in the surface seawater and compared with the microcosm incubation data. Subsequently, we used an ocean biogeochemical model to simulate the impact of aerosol N deposition on the primary production in the NWPO.

2. Materials and Methods

2.1. Collection of Haze Particles

Four aerosol samples were collected by the high-volume sampler (KC 1000, Qingdao, Laoshan Electric Inc., China) on 16 and 17 January 2014 (Haze-A), and 04-05, 03-04, and 02-03 December 2015 (Haze-B, Haze-C,

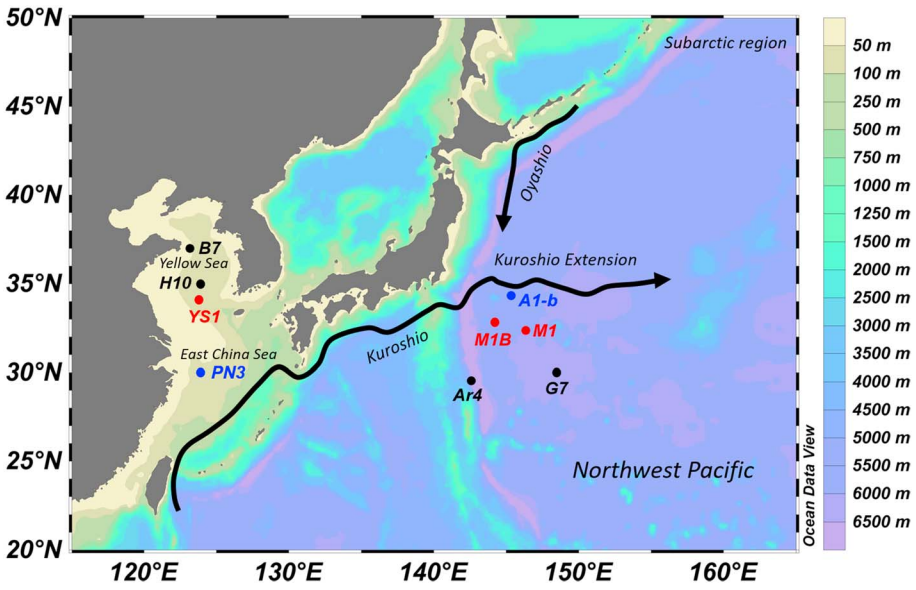

Figure 1. Locations of the sampling stations for microcosm experiments. Black, blue, and red represent experiments carried out in 2014, 2015, and 2016, respectively. The two black arrows represent the flow direction of *Kuroshio* and *Oyashio* currents. The background color shows the depth of the seawater.

and Haze-D) during pollution periods in Qingdao (120.49°E, 36.16°N), China (Table S1) in the. Samples were collected on quartz filters for ion analysis and Whatman®41 cellulose filters for trace metal analysis, respectively. The collected haze samples were stored frozen at −20 °C in the dark prior to use for chemical analysis and incubation experiments.

2.2. Microcosm Incubations

Nine sets of onboard microcosm experiments were performed on the *R/V Dongfanghong 2* spring 2014 (stations Ar4 and H10), 2015 (stations A1-b and PN3), and 2016 (stations YS1, M1, and M1B) cruises in the subtropical gyre of the NWPO (S-NWPO), YS (Yellow Sea), and ESC (East China Sea), respectively (Figure 1). At each station, surface seawater from the depth of 2–5 m was collected by Teflon-coated bottles (12 L) on a CTD (conductivity-temperature-depth) assembly (SeaBird 9/11, USA). After filtering through 200-μm Nylon mesh to remove larger zooplankton, filtered seawater with six (nine in 2014) different additions to triplicate microcosm experiments (duplicate in 2014) was transferred uniformly into acid washed 20-L polycarbonate bottles. Haze samples were dissolved into 60-mL deionized water (18.2 MΩ cm), sonicated for 1 hr at 0 °C. The suspensions were then added uniformly to incubation bottles. An on deck flow-through water bath was used to keep the temperature of incubation systems (i.e., three large plastic vessels) stable. The incubation microcosms were carried out under ambient light in 2014 and covered by neutral density screen to attenuate the light intensity by ~40% in 2015 and 2016 (Guo et al., 2012). The detailed water sampling scenario was given in Table S2.

Our incubation microcosms include the following:

1. Control: no additions;
2. Low haze particle loading: < 0.1 mg/L, simulating a typical aerosol case of at most 1 g m^{-2} into the upper 10-m layer of the water column (Guo et al., 2012; Iwamoto et al., 2011);
3. Medium loading: 0.1–0.6 mg/L, simulating a strong aerosol case of 1–6 g/m^2 into the upper 10-m layer of the water column (Guo et al., 2012; Mills et al., 2004);
4. High loading: 2 mg/L, simulating an extraordinarily strong aerosol case of 20 g/m^2 depositing into the upper 10-m layer of the water column (Table S3, Liu et al., 2013; Shi et al., 2012).

We also added a series of individual or combined nutrients to determine the nutrient limitation status of the seawater; details are given in Text S1 and Table S4.

Table 1
Baseline Conditions of the Sampling Stations

	Ar4	G7	M1B	A1-b	M1	H10	B7	YS1	PN3
Sampling date	2014.3.23	2014.4.5	2016.4.18	2015.4.18	2016.3.28	2014.4.29	2014.5.9	2016.3.22	2015.4.1
Incubation time	10 days	9 days	5 days	5 days	5 days	9 days	10 days	5 days	5 days
Sampling location	29.5°N, 142.5°E	30.0°N, 148.5°E	32.8°N, 144.2°E	34.2°N, 145.2°E	32.4°N, 146.3°E	35.0°N, 124.0°E	37.00°N, 123.17°E	34.0°N, 123.9°E	30.0°N, 124.0°E
Location	S-NWPO	S-NWPO	S-NWPO	S-NWPO	S-NWPO	YS	YS	YS	ECS
Temperature(°C)	18.9	18.3	19.0	18.4	18.5	12.6	9.8	11.2	13.8
Trophic state	TS-I	TS-I	TS-I	TS-I	TS-I	TS-II	TS-II	TS-II	TS-II
Chl *a* (μg/L)	0.24	0.50	0.50	0.43	0.76	2.74	1.58	0.92	8.61
NO_3^- +NO_2^- (μmol/L)	0.26	0.04	0.11	0.20	0.79	0.28	3.20	10.70	2.81
PO_4^{3-}(μmol/L)	0.05	0.05	0.053	0.061	0.095	0.04	0.10	0.667	0.022
N/P (μmol:μmol)	5	<1	2	3	8	7	32	16	>16
Microphytoplankton Chl *a* (%)	6	8	7	9	14	27	14	2	76
Nano-phytoplankton Chl *a* (%)	18	19	22	11	21	37	36	21	16
Pico-phytoplankton Chl *a* (%)	76	73	71	80	65	36	50	77	8

2.3. Chl *a* Concentration Measurement

A 300 mL of seawater was collected from the cultures at a preset time (8:00 a.m. everyday) and then sequentially filtered through 20-, 2- and 0.2-μm pore size membrane filters. The pigments on the filters were extracted in 90% acetone at −20 °C overnight, and fluorescence was measured on a Turner Trilogy fluorometer (Strickland & Parsons, 1972). Total Chl *a* concentration was obtained as the sum of those of all size fractions.

2.4. Chemical Analysis

Leachable nutrients (NO_3^-, NO_2^-, NH_4^+, and PO_4^{3-}) in the haze samples were extracted in an ultrasonic bath using deionized water for 1 hr at 0 °C (Liu et al., 2013). This method characterized by a high recovery has been widely used in determining soluble nutrients and trace metals in aerosol samples (Chen et al., 2006; Morton et al., 2013; Qi et al., 2018). The extracts were filtered through 0.45-μm PTFE syringe filters and then determined immediately. To determine the nutrient concentrations in seawater from the microcosm incubations, 200 mL of seawater was retrieved every day and filtered through preacid washed cellulose acetate membranes. The filtrates were then frozen and stored at −20 °C in acid-washed high-density polyethylene bottles until further analysis. QuAAtro (incubations in 2014) and AA3 (incubations in 2015 and 2016) Continuous Flow Analyzers (SEAL Analytical) were used to determine the nutrient concentrations following the automated colorimetric technique (Grasshoff et al., 1999). Detection limits of QuAAtro (AA3), defined as three times the standard deviation of the blanks, were 30 (20), 7 (5), 80 (40), and 40 (15) nmol/L for NO_3^-, NO_2^-, NH_4^+ and PO_4^{3-}, respectively.

The extraction of soluble trace metals in haze samples was similar to that of nutrients. After filtrating 0.45-μm polycarbonate membrane, the extraction was acidified to 1% with HNO_3 (ultrapure grades) and kept in 4 °C until analysis; A high-pressure digestion method was used to determine total trace metals in haze samples; details can be seen in the Hsu et al. (2010). Detection limit, recovery yield, and accuracy are summarized in Table S5.

2.5. Numerical Modeling

The Integrated Massively Parallel Atmospheric Chemical Transport model was used to simulate aerosol deposition rates in the NWPO during the winter and spring time in 2014 (Ito et al., 2018, and references therein). The model successfully simulated the bulk dissolved inorganic nitrogen (DIN) deposition at Qingdao (Ito et al., 2014; Zhang et al., 2008). The 3D-North Pacific Ecosystem Model Understanding Regional Oceanography was used for ocean biogeochemistry modeling. The model is coupled with a global physical ocean general circulation model COCO version 4.9 (Model for Interdisciplinary Research on Climate, Hasumi, 2006; Tatebe & Hasumi, 2010). The atmospheric model provided input data set of atmospheric nitrate and ammonium (in gas and aerosol phases) deposition. Further details of the model simulations are described in the Text S2.

Table 2
Dissolved Inorganic Nutrients and Trace Metals Leached From Haze Particulate Samples Used in This Study

	Nutrients (μmol/g)				Dissolved trace metals (μg/g) and solubility (in brackets)						
	NO_3^-	NO_2^-	NH_4^+	PO_4^{3-}	Pb	Cu	Cd	As	Co	Fe	Mn
Haze-A	2520	45.0	3840	2.0	156.9 (54%)	37.2 (38%)	1.3 (37%)	6.1 (37%)	0.8 (34%)	139.6 (2%)	156.5 (65%)
Haze-B	2400	9.1	6173	4.9	37.8 (16%)	52.2 (36%)	3.8 (61%)	22.2 (51%)	1.0 (27%)	98.3 (1%)	137.2 (51%)
Haze-C	4827	7.5	7624	9.7	103.2 (16%)	91.8 (30.9%)	12.6 (59%)	53.1 (40%)	2.2 (19%)	194.1 (1%)	323.1 (48%)
Haze-D	2923	154.2	4688	6.8	43.0 (9%)	68.2 (25%)	4.6 (32%)	46.4 (61%)	1.8 (17%)	167.1 (1%)	353.2 (51%)

2.6. Protocol of Data Analysis

One-way analysis of variance was used to assess if there is a significant difference in the mean of Chl *a* concentration among various treatments with Statistical Product and Service Solutions software.

3. Results

3.1. Baseline Conditions of Oceanic Water at the Sampling Stations

Location and trophic state of sampling stations is shown in Figure 1 and Table 1, respectively. Low concentrations of macronutrients ($NO_3^- + NO_2^- < 0.80$ μmol/L, $PO_4^{3-} < 0.10$ μmol/L) and Chl *a* (< 0.80 μg/L) were observed at stations Ar4, G7, M1, M1B, and A1-b in the S-NWPO. Chl *a* concentration was only 0.92 μg/L at station YS1 in the Yellow Sea, but the $NO_3^- + NO_2^-$ and PO_4^{3-} concentrations reached 10.7 and 0.67 μmol/L, respectively. Higher macronutrients or Chl *a* concentrations were also observed at stations H10 and B7 in the Yellow Sea and PN3 in the ECS. These results suggest a higher trophic state in the China coastal seas compared with the S-NWPO. On basis of these data, we divide the nine stations in our study into two classes: trophic state I (hereafter, TS-I) stations in the S-NWPO, including Ar4, G7, M1, M1B, and A1-b, and trophic state II (Hereafter, TS-II) stations in the China coastal seas, including H10, B7, YS1, and PN3 (Table 1).

Phytoplankton size structure, characterized by Chl *a* concentrations, displayed a concentration pattern of pico-size (0.2–2 μm) > nano-size (2–20 μm) > micro-size (>20 μm) at TS-I stations (Table 1). Pico-sized cells contributed 65–80% to total Chl *a* at TS-I stations. The contribution of pico-sized cells to total Chl *a* varied largely at TS-II stations, ranging from 8 to 77%.

Determining nutrient limiting conditions at each sampling station is essential to understand the role of nutrient supplied by aerosol deposition in affecting phytoplankton growth. According to the nutrient addition experiments and initial ratios of N:P in the collected seawater, the phytoplankton were under (1) N limitation at M1 (TS-I), M1B (TS-I), A1-b (TS-I), and H10 (TS-II); (2) P limitation at B7 (TS-II) and PN3 (TS-II); (3) NP colimitation at Ar4 (TS-I) and NPFe colimitation at G7 (TS-I); (4) no limitation at YS1 (TS-II, details in Text S3 and Figures S1–S3). In general, phytoplankton at TS-I stations in the S-NWPO were found to be limited by N or colimited by N and other nutrients (e.g., P and Fe). This is consistent with the result of previous studies that N is the primary limiting nutrient in this region (Kim et al., 2014; Li et al., 2015; Zhang et al., 2018). Indeed, the tendency toward nitrogen limitation prevails in the oligotrophic or less oligotrophic waters due to the higher acclimatization mechanisms of phytoplankton for coping with phosphorus rather than nitrogen stress (Moore et al., 2013). At TS-II stations in the China coastal seas, phytoplankton tend to be limited alone by N or P as a result of considerable riverine input and atmospheric deposition with a ratio of N:P > 16 (Chu et al., 2018; Liu et al., 2013; Shi et al., 2012; Wang et al., 2003), as well as frequent occurrence of phytoplankton bloom with a stoichiometric ratio of N:P < 16 (Arrigo, 2005; Zhang et al., 2018).

3.2. Composition of Haze Particles

Contents of nutrient and trace metals in the four aerosol samples vary mostly within a factor of 2–3 (Table 2). For example, the content of DIN (that is, $NO_3^- + NO_2^- + NH_4^+$) ranges from 6,405 to 12,458 μmol/g. This is much higher than those in mineral aerosols (Chu et al., 2018; Liu et al., 2013; Paytan et al., 2009; Shi et al., 2012) but similar to those in aerosols from other major Chinese cities (Du et al., 2011; Han et al., 2016; Tan et al., 2009). N/P ratios in the samples were larger than 16, which is similar to those aerosols reported in previous studies (Guo et al., 2012; Liu et al., 2013). Concentrations of $NO_3^- + NO_2^-$ from added haze particles

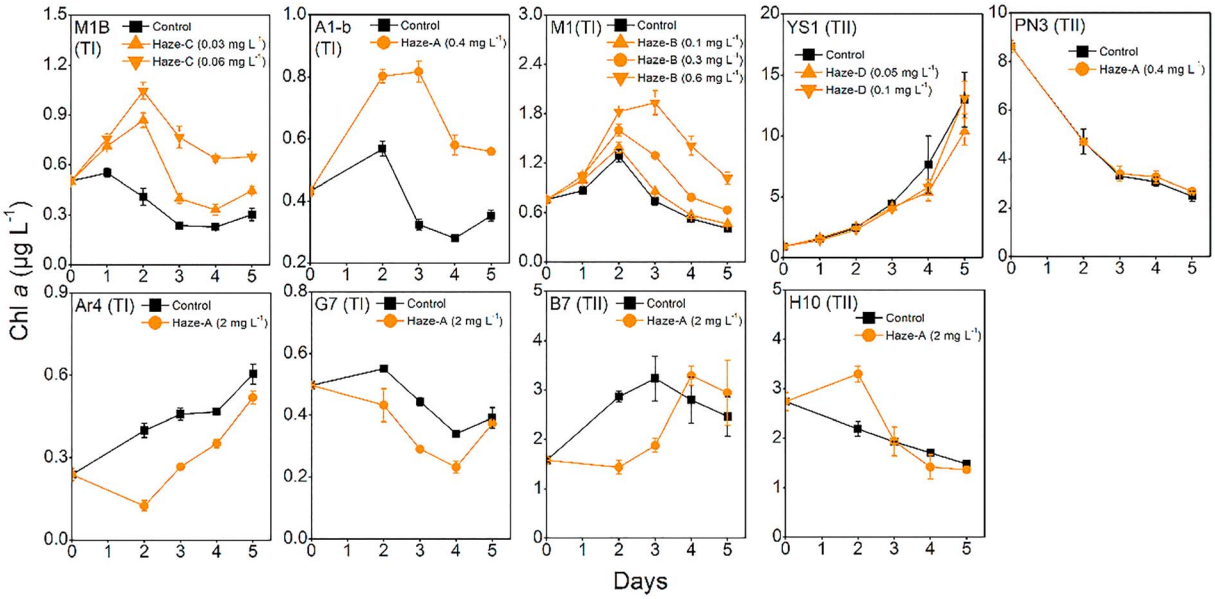

Figure 2. Responses of total Chl *a* to haze particle additions at different stations. At stations M1, M1B, and A1-b, addition of haze particles led to an increase in Chl *a* and enhancement increases with increasing haze particle loading (up to 0.6 mg/L) in comparison to controls. YS1 and PN3 showed no response to haze particle additions while higher particle loading (2 mg/L) caused a decrease in Chl *a* at all studied stations (Ar4, G7, B7, and H10) in comparison to controls—suggesting a toxicity effect.

ranged from 0.15 to 5.1 μmol/L in the incubated seawaters. The dissolved P from the added particles were < 5 nmol/L in all microcosms, which were negligible compared to the initial P stocks in the collected seawaters (Table S3). Trace metals in the samples generally had higher solubility than that of mineral aerosols (Mahowald et al., 2018), and dissolved trace metals added to the cultures were at least 1 order of magnitude higher than the stocks in the surface seawater of North Pacific Ocean (Table S3, Nozaki, 1997).

3.3. Responses of Phytoplankton to Low and Medium Haze Particle Additions

Chl *a* concentrations in the cultures at M1 (TS-I) increased with aerosol (Haze-B) loadings from 0.1 to 0.6 mg/L (Figure 2). Chl *a* in the 0.1-mg/L incubations was only slightly higher than in controls, but those in the 0.3 and 0.6 mg/L incubations were significantly higher ($p < 0.05$, during 3–5 days). Sized-fractionated Chl *a* showed positive responses to Haze-B additions and increased with cell size (Figure 3). In order to illustrate the shifts of phytoplankton size structure, we introduced the relative change in size-fractionated Chl *a* (e.g., $RC_{MChl\ a}$, $RC_{NChl\ a}$, and $RC_{PChl\ a}$ indicate the relative change in micro-, nano-, and pico-sized cells, respectively):

$$RC_{Chl\ a} = \frac{Chl\ a_T - Chl\ a_C}{Chl\ a_C} \times 100\%$$

where Chl a_T and Chl a_C represent the size-fractionated Chl *a* concentrations during the incubation experiment in the treatments and the control (μg/L), respectively. As a result, $RC_{MChl\ a}$ in Haze-B treatments at M1 was mainly distributed (25th-75th percentiles) from 9% to 35% at 0.1 mg/L, 26% to 128% at 0.3 mg/L, and 50% to 292% at 0.6 mg/L, respectively.

Significant increases in Chl *a* to low and medium loading haze particle additions were also observed at M1B (TS-I, $p < 0.05$, during 1–5 days) and A1-b (TS-I, $p < 0.05$, during 2–5 days). At M1B, $RC_{Chl\ a}$ in different sizes showed similar pattern compared with those at M1 (Figure 3). The most distinct size-dependent responses at M1B were observed in the micro-sized cells with the main distributions in $RC_{MChl\ a}$ from 79% to 135% at 0.03 mg/L, and 175% to 349% at 0.06 mg/L. At A1-b, all sized Chl *a* concentrations showed positive responses to the low addition of Haze-A, and $RC_{MChl\ a}$ was mainly distributed between 57% and 116% (Figure 3).

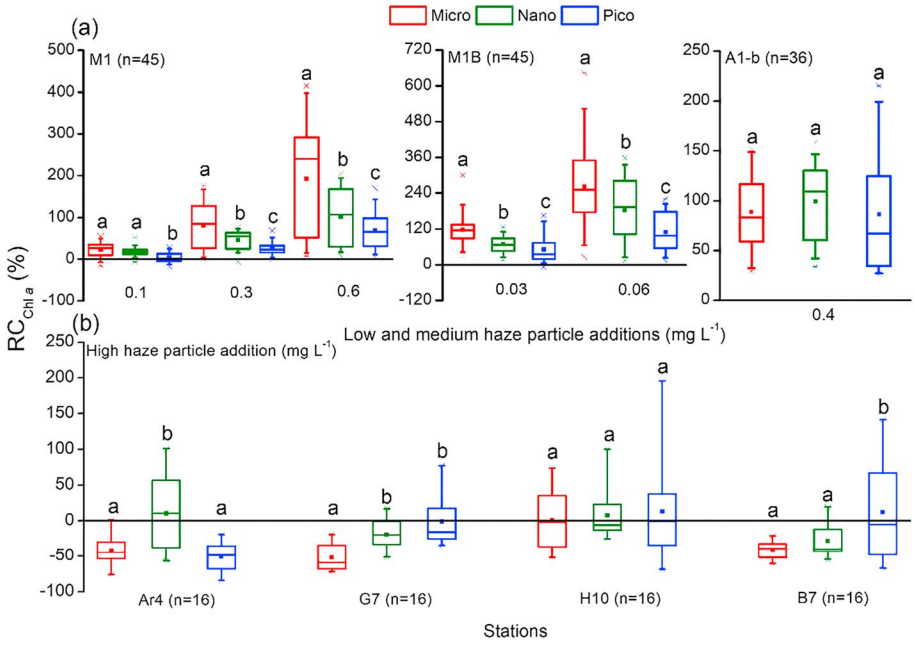

Figure 3. Box chart of relative change ($RC_{Chl\ a}$) in size-fractionated Chl *a* in the (a) low and medium ($n = 45, 36$), and (b) high ($n = 16$) haze particle additions during the incubation experiment at each station. The line across the boxes represents the 25th (bottom), 50th (middle), and 75th (top) percentiles, respectively; the whisker caps represent 5th and 95th percentiles; asterisks represent the minimum and maximum values; solid squares represent the mean values in each box. $RC_{Chl\ a}$ in various size-fractions that are significantly different are labeled with different letters ($p < 0.05$). For example, the $RC_{Chl\ a}$ in two sizes labeled with the same letter "a" means no significant difference between them, different letters "a" and "b" mean significant difference between them.

Two extreme cases were observed in the incubation experiments at YS1 and PN3 (TS-II). At YS1, Chl *a* concentration increased by about fourteen-fold to 12.97 μg/L at the end of the incubations compared to the initial value of 0.92 μg/L. In contrary, the mortality of phytoplankton prevailed during the control experiments at PN3. The initial Chl *a* concentration in the collected seawater at PN3 was as high as 8.61 μg/L but decreased to 2.48 μg/L at the end of the incubations. These results indicated that phytoplankton in the collected seawaters at YS1 and PN3 were at the beginning and end of blooms, respectively. For all haze particle additions at YS1 (0.05 and 0.1 mg/L) and PN3 (0.4 mg/L), no significant difference in Chl *a* was observed compared to the controls ($P > 0.05$, Figure 2).

3.4. Responses of Phytoplankton to High Haze Particle Additions

The response of phytoplankton to high haze particle additions (2 mg/L of Haze-A) can be divided into two patterns.

Pattern I Negative effect overall. Chl *a* concentrations were generally lower than those in the controls over the duration of the incubation experiments, as observed at Ar4 (TS-I), G7 (TS-I), and B7 (TS-II). In particular, Chl *a* showed significant difference ($p < 0.05$) and was 21–69% less than those in the controls during days 2 and 3. Size-fractionated Chl *a* generally showed negative responses to the haze particle additions. Especially for micro-sized cells, $RC_{MChl\ a}$ was generally below zero at the three stations (Figure 3).

Pattern II Complex response. Chl *a* concentrations were initially higher but then lower than those in the controls, as observed at H10 (TS-II). Chl *a* concentration increased to 3.30 μg/L on day 2, which was around 1.5-fold higher than those in the controls. However, this value was only 76% of that in N treatment (Figures 2 and S3), even though the added NO_3^- + NO_2^- in high haze loadings was 2.6-fold larger than the latter, suggesting a combined effect in high haze loadings occurred at H10. No obvious shift of phytoplankton size structure was observed at H10 (Figure 3).

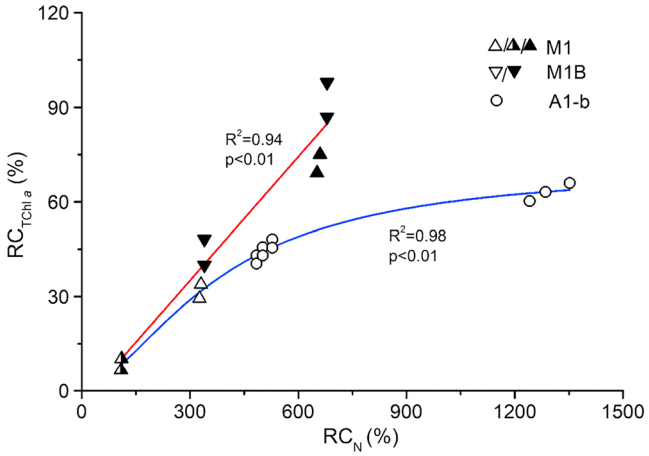

Figure 4. Correlations between $RC_{TChl\ a}$ and RC_N in haze particle (low and/or medium loadings at stations M1, M1B and A1-b) and nutrient (Cu + N and N + P at A1-b) treatments. Solid symbols were used for linear fitting, open symbols were used for nonlinear fitting, and semisolid symbols were shared by both fitting methods. Added N led to an increase in $RC_{TChl\ a}$ at A1-b but there was a surplus of $NO_3^- + NO_2^-$ (~0.35 μmol/L) at the end of the incubation experiments, suggesting that the N supplied by Haze-A reversed the nutrient limitation of the phytoplankton.

4. Discussion

4.1. Inhibition of Phytoplankton Growth at High Haze Particle Loadings

Our microcosm experiments demonstrated that haze particles at a loading of 2 mg/L had an inhibition effect on the growth of phytoplankton at stations Ar4 (TS-I), G7 (TS-I), B7 (TS-II), and H10 (TS-II, Figure 2). NO_3^- and NO_2^- were under used in the cultures at all four stations (Figure S4), which is likely the direct outcome of the toxicity effects. What caused the inhibition effect remains contentious. Heavy metals such as Cu have been suggested to inhibit phytoplankton growth (Jordi et al., 2012; Paytan et al., 2009). In our incubations, the ratio of added total Cu (from Haze-A) to total Chl *a* (unit: μg/μg) was 0.81, 0.39, 0.07, and 0.12 at Ar4, G7, H10, and B7, respectively. The ratio at Ar4 and G7 is higher but that at H10 and B7 is lower than the toxicity threshold of 0.2–2 μg/μg proposed by Paytan et al. (2009). Note that the calculated Cu toxicity threshold in this study is likely lower than that in realistic condition because the leaching treatment at 0 °C may induce less release of soluble Cu from haze particles. To further test whether it is the Cu that caused the toxicity effect in the NWPO, we added soluble Cu and N to incubations at A1-b. The calculated Cu to initial Chl *a* ratio is 0.25 μg/μg, which is higher than the Cu toxicity threshold (Paytan et al., 2009). But we did not see an inhibition effect (Figure S2). This suggests that either other toxins induced the toxicity to phytoplankton or the Cu toxicity threshold may deviate from that in the H10, B7, and A1-b stations because of the varying phytoplankton species. The initial stimulation effects at H10 (Figure 2) may be related to the ambient seawater conditions. The high Chl *a* at H10 is usually associated with high organic matter content in the seawater, which might have a mediating effect on the toxicity of haze particle to phytoplankton (Fisher & Frood, 1980). Different Fe stocks in the incubated seawater may also affect the toxicity of Cu on phytoplankton (Paytan et al., 2009; Wang et al., 2017). Considering the high concentrations of toxic substances such as Cu, Pb, and Cd in the incubated seawaters amended with high haze particle additions, the toxicity may be a synergistic effect of multiple toxic substances (Miao et al., 2005). In addition, although we did not determine the content of organic compounds in haze particles, the reported toxicity of organic pollutants such as pyrene and phenanthrene on phytoplankton may not be ignored (Echeveste et al., 2010).

4.2. No Observed Effect of Haze Particles on Phytoplankton Growth at YS1 and PN3 Stations

The addition of low and medium loadings of haze particles at YS1 (TS-II) and PN3 (TS-II) did not induce significant changes in Chl *a* compared with the controls (Figure 2). This is likely related to the two extreme physiological states of the phytoplankton during the incubation experiments: exponential growth phase at YS1 and decline phase at PN3. In the exponential growth phase at YS1, the addition of Haze-D had no observable effects on phytoplankton growth due to the negligible supply of nutrients as well as the relatively nutrient-saturated baseline environment. In the declining phase at PN3, the supplied P of 8 nmol/L by Haze-A was not enough to satisfy the demands of phytoplankton community, especially for large-sized cells with a higher demand of nutrients compared with the pico-sized cells (Maranon et al., 2007).

4.3. Fertilization Effect of Haze Particles on Phytoplankton Growth at Low-Medium Loadings

The N/P ratio in the haze particles (>1,000) is much higher than the Redfield ratio (N/P=16), which indicated the importance and potential impact of anthropogenic pollutant deposition as a source of nitrogen to the S-NWPO and China coastal seas [Kim et al., 2014]. Our results clearly demonstrated that low and medium loadings of haze particles in the incubations generally stimulated phytoplankton growth. As phytoplankton at M1, M1B, and A1-b (TS-I) were primarily limited by N, we plotted the relative change of inorganic N (RC_N) to that of Chl *a* ($RC_{TChl\ a}$) to quantify the N fertilization impact of haze particle additions. Relative change in DIN, RC_N, reflects the magnitude of DIN input to the baseline value and is defined as

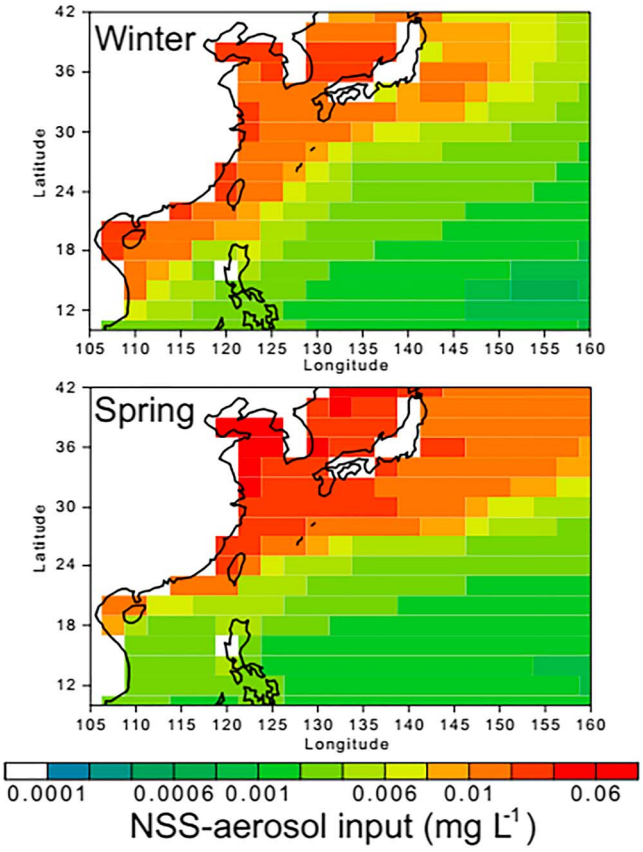

Figure 5. Maximum 10-day accumulated concentration of total suspended particle (non-sea-salt aerosol) in the surface ocean of NWPO estimated from modeled daily average fluxes in the winter and spring in 2014. Highest loading was seen in China coastal seas. Particle loading at the open ocean in NWPO is usually substantially less than 0.06 mg/L.

$$RC_N = \frac{N_T - N_B}{N_B} \times 100\%$$

where N_T represents the input of DIN (μmol/L) and N_B represents the baseline values in the initial collected seawater (μmol/L).

In general, the relationship between $RC_{TChl\ a}$ and RC_N can be divided into two types (Figure 4): (1) linear increase. In this type, the NO_3^- + NO_2^- concentration in the cultures after haze particle additions was nearly exhausted at the end of the incubations at M1 and M1B (Figure S5); (2) nonlinear increase. There was a surplus of NO_3^- + NO_2^- (~0.35 μmol/L) at the end of the incubation experiments (e.g., A1-b), suggesting the N supplied by Haze-A reversed the nutrient limitation of the phytoplankton. Overall, the addition of haze particle supplies a considerable amount of N nutrients to relieve and even reverse the nutrient limitation of phytoplankton community. Although we cannot exclude the possible stimulation effects of other species, such as Cu (Meng et al., 2016), our results suggest a dominant role of nitrogen in aerosol in affecting phytoplankton in the primarily N-limited NWPO.

At M1, M1B, and A1-b, although the pico-sized cells are the dominant contributor to total Chl *a* in the baseline seawaters, micro-sized and nano-sized cells showed larger responses to haze particle additions. Thus, the phytoplankton size structure shifts toward larger cells during the incubation experiments. This phenomenon was observed in previous incubation experiments with nutrient enrichments (Guo et al., 2012; Hoffmann et al., 2006; Liu et al., 2013; Zhang et al., 2018). Pico-sized cells with larger surface area/volume ratios generally have a competitive advantage for adapting the nutrient limiting environments. In contrary, when the nutrients were sufficient to support all sized phytoplankton, micro-sized and nano-sized cells usually show more rapid growth. This is attributed to their own higher photosynthetic efficiency (Maranon et al., 2007) and an ability of taking up excess nutrients for sustaining their growth (Falkowski et al., 1998). In particular, in the spring, substantial aerosol nutrient supply as well as suitable environmental conditions (e.g., temperature and sunlight intensity) had the potential to induce bloom dominated by larger-sized cells (Guo et al., 2012; Liu et al., 2013; Zhang et al., 2018).

4.4. Deposition Flux of Haze Particle and Its Impact on Chl *a* Concentrations and Primary Productivity in the NWPO

Collectively, the above results showed that aerosol toxicity to phytoplankton under different trophic states in the NWPO only occurred at high haze particle loadings (2 mg/L) but not at low and medium loadings (0.03–0.6 mg/L). Thus, the aerosol loadings are important to evaluate their overall effect on phytoplankton growth in the NWPO. Daily depositing fluxes of non-sea-salt aerosols in the winter (December-January-February) and spring (March-April-May) with frequent haze events in 2014 were estimated from the Integrated Massively Parallel Atmospheric Chemical Transport model (Ito et al., 2018). By assuming a minimum surface mixed layer depth of 10 m (Martino et al., 2014; Paytan et al., 2009) and a residence time of 10 days (Text S4), we estimated the cumulative mass loadings of non-sea-salt aerosols (representing haze particles) in the surface seawater of the NWPO. The maximum concentration of non-sea-salt aerosols over any 10-day period in December-January-February and March-April-May of 2014 was shown in Figure 5. The estimated maximum mass concentration of non-sea-salt particles was ~0.05 mg/L in the winter and 0.33 mg/L in the spring, respectively (Figure 5). The higher loadings in the spring were influenced by haze as well as dust storm events (Shi et al., 2012). In all cases, mass loading of non-sea-salt aerosol particles was substantially lower than 0.06 mg/L in the open ocean of the NWPO. It is possible that soluble trace metals such as Cu may accumulate in the upper ocean after particle deposition over a relatively long time (e.g., months),

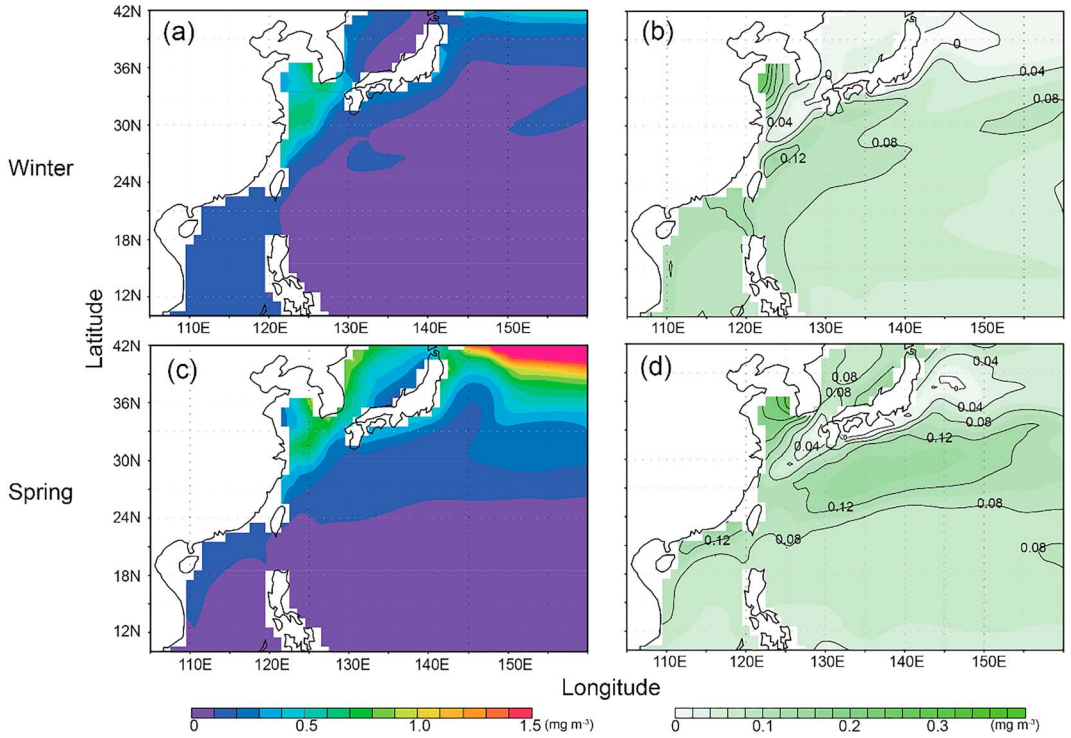

Figure 6. Modeled surface Chl *a* concentrations (a and c) without N deposition (simulated from the IMPACT model) and modeled difference in surface Chl *a* concentrations with and without N deposition (b and d). In both seasons, deposited N enhanced Chl *a* in surface oceans. IMPACT = Integrated Massively Parallel Atmospheric Chemical Transport.

which has a potential to cause toxicity to phytoplankton. However, during the residence time of most trace metals, they will gradually be complexed with organic matters in the seawater, which would reduce, even prevent, the potential toxicity on phytoplankton (Sunda, 2012). For instance, due to the river input and atmospheric deposition, the ECS is regarded as the area characterized by relatively high levels of Cu in the surface seawater. However, microcosm incubation experiments conducted in the ECS showed that Cu in the aerosol might play a more important role in stimulating primary productivity than N, likely due to the high biomass in the ECS (Meng et al., 2016). Hence, combined with the modeling and above experimental results, we conclude that the deposition of haze particles in natural condition tends to cause a fertilization rather than inhibition effect on primary productivity over the NWPO.

The estimation of cumulative loadings of haze particles in our study was based on the total atmospheric deposition including wet and dry deposition. Although the dry deposition characterized by accumulated input of haze particles, as well as wet deposition characterized by short-term considerable input of haze particles, may have different impact on phytoplankton growth and community structure (Liu et al., 2013; Zhang et al., 2019), the general fertilization impact would not be changed. Similarly, the heterotrophic organisms such as heterotrophic nanoflagellate and bacteria are very likely to show similar responses to the addition of haze particles (Guo et al., 2012; Maranon et al., 2010). But the threshold causing an inhibition impact on heterotrophic organisms may be different from that on phytoplankton. Hence, the overall impact of anthropogenic aerosol deposition on marine ecosystems still needs to be further investigated.

In our onboard incubation experiments, we showed that the fertilization effects of haze particles on phytoplankton growth are mainly from their dissolved N. On this basis, we used an ocean biogeochemical model to estimate the impact of nitrogen deposition on Chl *a*, compared with a baseline model run without nitrogen deposition in the surface seawater of the NWPO during the winter and spring of 2014 (Figure 6). The 3D-North Pacific Ecosystem Model Understanding Regional Oceanography (Aita et al., 2007) simulations showed that monthly averaged Chl *a* concentration increased from 0.07 mg/m^3 without N deposition to 0.15 mg/m^3 with N deposition in the winter and from 0.15 mg/m^3 without N deposition to 0.25 mg/m^3

with N deposition in the spring, respectively. The increase in Chl *a* is consistent with previously modeled result in the Japan Sea (Onitsuka et al., 2009) and that in the NWPO (Taketani et al., 2018). Considering the important role of haze particle (regarded as a typical air pollutant) in transferring N from the continent to the ocean, as well as increasing anthropogenic influences on marine aerosols (Kim et al., 2014; Luo et al., 2018), our results indicate the crucial role of haze deposition on primary production in the NWPO.

The stimulation effect of N deposition on phytoplankton growth has the potential to enhance the capacity of carbon fixation in the ocean. Total N deposition is estimated to be 6 $Tg{\cdot}N{\cdot}year^{-1}$ in 2014 in the study area (Figure 5). Considering that the NWPO is generally N limited (Chu et al., 2018; Kim et al., 2014; Liu et al., 2013; Martino et al., 2014; Zhang et al., 2018), we estimate the primary productivity due to N deposition in the NWPO using the Redfield Ratio of C:N to be ~42 $Tg{\cdot}C{\cdot}year^{-1}$. We emphasize that the actual impact of the N deposition on the ocean ecosystems and primary productivity is highly complex, although our estimate is broadly consistently with that from Duce et al. (2008). For example, the actual impact of N deposition may be dependent on the timing of the deposition in relation to the different phases of the bloom as observed in the incubations YS1 and PN3. On the other hand, the input of N contributed to the accumulation of N in the seawater, which had a potential to induce blooms of large-sized phytoplankton, characterized by a higher carbon sequestration efficiency (Maranon et al., 2007). Further Earth system modeling needs to consider this aspect in order to quantify the impact of N deposition on primary production and carbon uptake (Kim et al., 2014). Finally, our results suggest that with the current control of nitrogen oxides emission in East Asia, we may see a decrease in primary productivity in NWPO if other conditions remain unchanged in the future.

Acknowledgments

This work was supported by National Natural Science Foundation of China (41876125; PI: Gao), Major State Basic Research Development Program of China (973 Program) (2014CB953701, PI: Gao); NSFC-Royal Society travel grant (41511130068, PIs Gao and Shi and NE/K000845/1: PI Shi); and UK Natural Environment Research Council (NE/I021616/1: PI Shi). Support for this research was provided to A. Ito and M. N. Aita by JSPS KAKENHI grants JP16K00530 and JP15H05822, respectively. A. Ito and M. N. Aita acknowledge financial support by Integrated Research Program for Advancing Climate Models (MEXT). The numerical simulations for atmospheric deposition were performed using the SGI ICE X and Earth Simulator 3 at the JAMSTEC. The GEOS data used in this study have been provided by the Global Modeling and Assimilation Office (GMAO) at NASA Goddard Space Flight Center. C. Z., H. G., and Z. S. designed the experiment; C. Z. and Q. C. performed the onboard experiments and laboratory tests; Z. S., A. I., and M. N. A. designed the modeling work and A. I. and M. N. A. performed the model simulations; J. S. designed the microcosm device and determined the contents of trace metals in particle matters; C. Z., H. G., Z. S., X. G., and X. Y. analyzed the data. All authors contributed to the manuscript drafting. The authors declare no competing financial interests. Relevant data are publically available at https://doi.org/10.25500/edata.bham.00000334.

References

Aita, M. N., Yamanaka, Y., & Kishi, M. J. (2007). Interdecadal variation of the lower trophic ecosystem in the northern Pacific between 1948 and 2002, in a 3-D implementation of the NEMURO model. *Ecological Modelling*, *202*(1-2), 81–94. https://doi.org/10.1016/j.ecolmodel.2006.07.045

Arrigo, K. R. (2005). Marine microorganisms and global nutrient cycles. *Nature*, *437*(7057), 349–355. https://doi.org/10.1038/nature04159

Boyd, P. W., Jickells, T., Law, C. S., Blain, S., Boyle, E. A., Buesseler, K. O., et al. (2007). Mesoscale iron enrichment experiments 1993-2005: Synthesis and future directions. *Science*, *315*(5812), 612–617. https://doi.org/10.1126/science.1131669

Chen, Y., Street, J., & Paytan, A. (2006). Comparison between pure-water-and seawater-soluble nutrient concentrations of aerosols from the Gulf of Aqaba. *Marine Chemistry*, *101*(1-2), 141–152. https://doi.org/10.1016/j.marchem.2006.02.002

Chu, Q., Liu, Y., Shi, J., Zhang, C., Gong, X., Yao, X., et al. (2018). Promotion effect of Asian dust on phytoplankton growth and potential dissolved organic phosphorus utilization in the South China Sea. *Journal of Geophysical Research: Biogeosciences*, *123*, 1101–1116. https://doi.org/10.1002/2017JG004088

Du, H., Kong, L., Cheng, T., Chen, J., Du, J., Li, L., et al. (2011). Insights into summertime haze pollution events over Shanghai based on online water-soluble ionic composition of aerosols. *Atmospheric Environment*, *45*(29), 5131–5137. https://doi.org/10.1016/j.atmosenv.2011.06.027

Duce, R., LaRoche, J., Altieri, K., Arrigo, K. R., Baker, A. R., Capone, D. G., et al. (2008). Impacts of atmospheric anthropogenic nitrogen on the open ocean. *Science*, *320*(5878), 893–897. https://doi.org/10.1126/science.1150369

Echeveste, P., Dachs, J., Berrojalbiz, N., & Agustí, S. (2010). Decrease in the abundance and viability of oceanic phytoplankton due to trace levels of complex mixtures of organic pollutants. *Chemosphere*, *81*(2), 161–168. https://doi.org/10.1016/j.chemosphere.2010.06.072

Falkowski, P. G., Barber, R. T., & Smetacek, V. (1998). Biogeochemical controls and feedbacks on ocean primary production. *Science*, *281*(5374), 200–206. https://doi.org/10.1126/science.281.5374.200

Fisher, N., & Frood, D. (1980). Heavy metals and marine diatoms: Influence of dissolved organic compounds on toxicity and selection for metal tolerance among four species. *Marine Biology*, *59*(2), 85–93. https://doi.org/10.1007/BF00405458

Gao, M., Guttikunda, S. K., Carmichael, G. R., Wang, Y., Liu, Z., Stanier, C. O., et al. (2015). Health impacts and economic losses assessment of the 2013 severe haze event in Beijing area. *Science of the Total Environment*, *511*, 553–561. https://doi.org/10.1016/j.scitotenv.2015.01.005

Grasshoff, K., Kremling, K., & Ehrhardt, M. (1999). Determination of nutrients. In *Methods of seawater analysis* (3rd ed.,pp. 159–223). New York: Wiley-VCH. https://doi.org/10.1002/9783527613984

Guo, C., Yu, J., Ho, T. Y., Wang, L., Song, S., Kong, L., & Liu, H. (2012). Dynamics of phytoplankton community structure in the South China Sea in response to the East Asian aerosol input. *Biogeosciences*, *9*(4), 1519–1536. https://doi.org/10.5194/bg-9-1519-2012

Han, B., Zhang, R., Yang, W., Bai, Z., Ma, Z., & Zhang, W. (2016). Heavy haze episodes in Beijing during January 2013: Inorganic ion chemistry and source analysis using highly time-resolved measurements from an urban site. *Science of the Total Environment*, *544*, 319–329. https://doi.org/10.1016/j.scitotenv.2015.10.053

Hasumi, H. (2006). CCSR Ocean Component Model (COCO) version 4.0, Rep. 25, Cent, for Clim. Syst. Res., University of Tokyo.

Hoffmann, L. J., Peeken, I., Lochte, K., Assmy, P., & Veldhuis, M. (2006). Different reactions of Southern Ocean phytoplankton size classes to iron fertilization. *Limnology and Oceanography*, *51*(3), 1217–1229. https://doi.org/10.4319/lo.2006.51.3.1217

Hsu, S., Liu, S. C., Arimoto, R., Shiah, F., Gong, G., Huang, Y., et al. (2010). Effects of acidic processing, transport history, and dust and sea salt loadings on the dissolution of iron from Asian dust. *Journal of Geophysical Research*, *115*, D19313. https://doi.org/10.1029/2009JD013442

Ito, A., Lin, G., & Penner, J. E. (2014). Reconciling modeled and observed atmospheric deposition of soluble organic nitrogen at coastal locations. *Global Biogeochemical Cycles*, *28*, 617–630. https://doi.org/10.1002/2013GB004721

Ito, A., Lin, G., & Penner, J. E. (2018). Radiative forcing by light-absorbing aerosols of pyrogenetic iron oxides. *Scientific Reports*, *8*(1), 7347. https://doi.org/10.1038/s41598-018-25756-3

Ito, A., Myriokefalitakis, S., Kanakidou, M., Mahowald, N. M., Scanza, R. A., Hamilton, D. S., et al. (2019). Pyrogenic iron: The missing link to high iron solubility in aerosols. *Science Advances*, *5*(5), eaau7671. https://doi.org/10.1126/sciadv.aau7671

Iwamoto, Y., Yumimoto, K., Toratani, M., Tsuda, A., Miura, K., Uno, I., & Uematsu, M. (2011). Biogeochemical implications of increased mineral particle concentrations in surface waters of the northwestern North Pacific during an Asian dust event. *Geophysical Research Letters*, *38*, L01604. https://doi.org/10.1029/2010GL045906

Jordi, A., Basterretxea, G., Tovar-Sanchez, A., Alastuey, A., & Querol, X. (2012). Copper aerosols inhibit phytoplankton growth in the Mediterranean Sea. *Proceedings of the National Academy of Sciences of the United States of America*, *109*(52), 21,246–21,249. https://doi.org/10.1073/pnas.1207567110

Kim, I. N., Lee, K., Gruber, N., Karl, D. M., Bullister, J. L., Yang, S., & Kim, T. W. (2014). Increasing anthropogenic nitrogen in the North Pacific Ocean. *Science*, *346*(6213), 1102–1106. https://doi.org/10.1126/science.1258396

Krom, M. D., Shi, Z., Stockdale, A., Berman-Frank, I., Giannakourou, A., Herut, B., et al. (2016). Response of the Eastern Mediterranean microbial ecosystem to dust and dust affected by acid processing in the atmosphere. *Frontiers in Marine Science*, *3*, 133. https://doi.org/10.3389/fmars.2016.00133

Li, Q., Legendre, L., & Jiao, N. (2015). Phytoplankton responses to nitrogen and iron limitation in the tropical and subtropical Pacific Ocean. *Journal of Plankton Research*, *37*(2), 306–319. https://doi.org/10.1093/plankt/fbv008

Li, W., Xu, L., Liu, X., Zhang, J., Lin, Y., Yao, X., et al. (2017). Aerosol–pollution interaction produces more soluble iron for the ocean ecosystems. *Science Advances*, *3*(3), e1601749. https://doi.org/10.1126/sciadv.1601749

Liu, Y., Zhang, T., Shi, J., Gao, H., & Yao, X. (2013). Responses of chlorophyll a to added nutrients, Asian dust, and rainwater in an oligotrophic zone of the Yellow Sea: Implications for promotion and inhibition effects in an incubation experiment. *Journal of Geophysical Research: Biogeosciences*, *118*, 1763–1772. https://doi.org/10.1002/2013JG002329

Luo, L., Kao, S. J., Bao, H., Xiao, H., Xiao, H., Yao, X., et al. (2018). Sources of reactive nitrogen in marine aerosol over the Northwest Pacific Ocean in spring. *Atmospheric Chemistry and Physics*, *18*(9), 6207–6222. https://doi.org/10.5194/acp-18-6207-2018

Mahowald, N. M. (2011). Aerosol indirect effect on biogeochemical cycles and climate. *Science*, *334*(6057), 794–796. https://doi.org/10.1126/science.1207374

Mahowald, N. M., Hamilton, D. S., Mackey, K. R. M., Moore, J. K., Baker, A. R., Scanza, R. A., & Zhang, Y. (2018). Aerosol trace metal leaching and impacts on marine microorganisms. *Nature Communications*, *9*(1), 2614. https://doi.org/10.1038/s41467-018-04970-7

Maranon, E., Cermeóo, P., Rodríguez, J., Zubkov, M. V., & Harris, R. P. (2007). Scaling of phytoplankton photosynthesis and cell size in the ocean. *Limnology and Oceanography*, *52*(5), 2190–2198. https://doi.org/10.2307/4502368

Maranon, E., Fernández, A., Mouriño-Carballido, B., MartÍnez-GarcÍa, S., Teira, E., Cermeño, P., et al. (2010). Degree of oligotrophy controls the response of microbial plankton to Saharan dust. *Limnology and Oceanography*, *55*(6), 2339–2352. https://doi.org/10.4319/lo.2010.55.6.2339

Martino, M., Hamilton, D., Baker, A. R., Jickells, T. D., Bromley, T., Nojiri, Y., et al. (2014). Western Pacific atmospheric nutrient deposition fluxes, their impact on surface ocean productivity. *Global Biogeochemical Cycles*, *28*, 712–728. https://doi.org/10.1002/2013GB004794

Meng, X., Chen, Y., Wang, B., Ma, Q., & Wang, F. (2016). Responses of phytoplankton community to the input of different aerosols in the East China Sea. *Geophysical Research Letters*, *43*, 7081–7088. https://doi.org/10.1002/2016GL069068

Miao, A., Wang, X., & Juneau, P. (2005). Comparison of Cd, Cu, and Zn toxic effects on four marine phytoplankton by pulse-amplitude-modulated fluorometry. *Environmental Toxicology and Chemistry*, *24*(10), 2603–2611. https://doi.org/10.1897/05-009r.1

Mills, M. M., Ridame, C., Davey, M., la Roche, J., & Geider, R. J. (2004). Iron and phosphorus co-limit nitrogen fixation in the eastern tropical North Atlantic. *Nature*, *429*(6989), 292–294. https://doi.org/10.1038/nature02550

Moore, C. M., Mills, M. M., Arrigo, K. R., Berman-Frank, I., Bopp, L., Boyd, P. W., et al. (2013). Processes and patterns of oceanic nutrient limitation. *Nature Geoscience*, *6*(9), 701–710. https://doi.org/10.1038/ngeo1765

Morton, P. L., Landing, W. M., Hsu, S. C., Milne, A., Aguilar-Islas, A. M., Baker, A. R., et al. (2013). Methods for the sampling and analysis of marine aerosols: Results from the 2008 GEOTRACES aerosol intercalibration experiment. *Limnology and Oceanography: Methods*, *11*(2), 62–78. https://doi.org/10.4319/lom.2013.11.62

Nozaki, Y. (1997). A fresh look at element distribution in the North Pacific. *EOS Transactions*, *78*(21), 221. https://doi.org/10.1029/97EO00148

Onitsuka, G., Uno, I., Yanagi, T., & Yoon, J. H. (2009). Modeling the effects of atmospheric nitrogen input on biological production in the Japan Sea. *Journal of Oceanography*, *65*(3), 433–438. https://doi.org/10.1007/s10872-009-0038-4

Paytan, A., Mackey, K. R., Chen, Y., Lima, I. D., Doney, S. C., Mahowald, N., et al. (2009). Toxicity of atmospheric aerosols on marine phytoplankton. *Proceedings of the National Academy of Sciences of the United States of America*, *106*(12), 4601–4605. https://doi.org/10.1073/pnas.0811486106.

Qi, J., Liu, X., Yao, X., Zhang, R., Chen, X., Lin, X., et al. (2018). The concentration, source and deposition flux of ammonium and nitrate in atmospheric particles during dust events at a coastal site in northern China. *Atmospheric Chemistry and Physics*, *18*(2), 571–586. https://doi.org/10.5194/acp-18-571-2018

Shi, J., Gao, H., Zhang, J., Tan, S., Ren, J., Liu, C., et al. (2012). Examination of causative link between a spring bloom and dry/wet deposition of Asian dust in the Yellow Sea, China. *Journal of Geophysical Research*, *117*, D17304. https://doi.org/10.1029/2012JD017983

Strickland, J. D. H., & Parsons, T. R. (1972). Pigment analysis. In *A practical handbook of seawater analysis* (3rd ed.,pp. 185–205). Ottawa: Fisheries Research Board of Canada.

Su, B., Zhan, M., Zhai, J., Wang, Y., & Fischer, T. (2014). Spatio-temporal variation of haze days and atmospheric circulation pattern in China (1961–2013). *Quaternary International*, *380-381*, 14–21. https://doi.org/10.1016/j.quaint.2014.11.044

Sunda, W. (2012). Feedback interactions between trace metal nutrients and phytoplankton in the ocean. *Frontiers in Microbiology*, *3*, 204. https://doi.org/10.3389/fmicb.2012.00204

Taketani, F., Aita, M. N., Yamaji, K., Sekiya, T., Ikeda, K., Sasaoka, K., et al. (2018). Seasonal response of north western Pacific marine ecosystems to deposition of atmospheric inorganic nitrogen compounds from East Asia. *Scientific Reports*, *8*(1), 9324. https://doi.org/10.1038/s41598-018-27523-w

Tan, J., Duan, J., Chen, D., Wang, X., Guo, S., Bi, X., et al. (2009). Chemical characteristics of haze during summer and winter in Guangzhou. *Atmospheric Research*, *94*(2), 238–245. https://doi.org/10.1016/j.atmosres.2009.05.016

Tatebe, H., & Hasumi, H. (2010). Formation mechanism of the Pacific equatorial thermocline revealed by a general circulation model with a high accuracy tracer advection scheme. *Ocean Model*, *35*(3), 245–252. https://doi.org/10.1016/j.ocemod.2010.07.011

Tie, X., Huang, R.-J., Dai, W., Cao, J., Long, X., Su, X., et al. (2016). Effect of heavy haze and aerosol pollution on rice and wheat productions in China. *Scientific Reports*, *35*, 29612. https://doi.org/10.1016/j.ocemod.2010.07.011

Wang, B., Wang, X., & Zhan, R. (2003). Nutrient conditions in the Yellow Sea and the East China Sea. *Estuarine, Coastal and Shelf Science*, *58*(1), 127–136. https://doi.org/10.1016/S0272-7714(03)00067-2

Wang, F., Chen, Y., Guo, Z., Gao, H., Mackey, K. R., Yao, X., et al. (2017). Combined effects of iron and copper from atmospheric dry deposition on ocean productivity. *Geophysical Research Letters*, *44*, 2546–2555. https://doi.org/10.1002/2016GL072349

Zhang, B., Wang, Y., & Hao, J. (2015). Simulating aerosol-radiation-cloud feedbacks on meteorology and air quality over eastern China under severe haze conditions in winter. *Atmospheric Chemistry and Physics*, *15*(5), 2387–2404. https://doi.org/10.5194/acp-15-2387-2015

Zhang, C., Gao, H., Yao, X., Shi, Z., Shi, J., Yu, Y., et al. (2018). Phytoplankton growth response to Asian dust addition in the northwest Pacific Ocean versus the Yellow Sea. *Biogeosciences*, *15*(3), 749–765. https://doi.org/10.5194/bg-15-749-2018

Zhang, C., Yao, X., Chen, Y., Chu, Q., Yu, Y., Shi, J., & Gao, H. (2019). Variations in the phytoplankton community due to dust additions in eutrophication, LNLC and HNLC oceanic zones. *Science of the Total Environment*, *669*, 282–293. https://doi.org/10.1016/j.scitotenv.2019.02.068

Zhang, Y., Liu, X. J., Fangmeier, A., Goulding, K. T. W., & Zhang, F. S. (2008). Nitrogen inputs and isotopes in precipitation in the North China Plain. *Atmospheric Environment*, *42*(7), 1436–1448. https://doi.org/10.1016/j.atmosenv.2007.11.002

Zhao, Y., Zhang, J., & Nielsen, C. P. (2012). The effects of recent control policies on trends in emissions of anthropogenic atmospheric pollutants and CO_2 in China. *Atmospheric Chemistry and Physics*, *13*(2), 487–508. https://doi.org/10.5194/acp-13-487-2013

Erratum

The Supporting Information files originally published with this article were outdated and were not the final version intended for publication. The originally-published files have been replaced with the correct files, and this may be considered the official version of record.